INTERNATIONAL JOURNAL OF PRECISION ENGINEERING AND MANUFACTURING Vol. 17, No. 9, pp. 1175-1185 SEPTEMBER 2016 / 1175
DOI: 10.1007/s12541-016-0141-6 ISSN 2234-7593 (Print) / ISSN 2005-4602 (Online)

Performance Optimization of Dielectric Electro Active Polymers in Wave Energy Converter Application

Phan Cong Binh[1] and Kyoung Kwan Ahn[1,#]

1 School of Mechanical Engineering, University of Ulsan, Daehakro 93, Namgu, Ulsan, 44610, South Korea
Corresponding Author / E-mail: kkahn@ulsan.ac.kr, TEL: +82-52-259-2282, FAX: +82-52-259-1680

KEYWORDS: Dielectric electro active polymer, WEC, Stretch ratio control, Supplementary inertia

This paper presents a design, modeling and control of a novel wave energy converter (WEC) using Dielectric electro active polymer (DEAP). Application of DEAP in WEC has attracted a lot of works due to development of renewable energy and increasing of human energy demand. However, various challenges of the WEC using DEAP must be overcome before going to realistic application. Firstly, stretch ratio has significant influence on energy conversion efficiency of DEAP. It cannot exceed the limitation value due to mechanical or electrical breakdown, whereas small stretch ratio reduces the energy conversion efficiency significant. Secondly, WEC has to be controlled to maximize the absorbed energy. Therefore, this study employs an innovative device which can adjust the inertia of the floating buoy. A variable inertia hydraulic flywheel is attached on the main thrust shaft to control stretch ratio based on change in the hydrodynamic behavior of the system. A proportional–integral–derivative (PID) controller is designed to optimize stretch ratio under different regular waves. Consequently, the overall energy conversion efficiency of the proposed WEC can reach up to 25%.

Manuscript received: January 21, 2016 / Revised: April 21, 2016 / Accepted: May 12, 2016

NOMENCLATURE

a = Buoy radius
A = Wave amplitude
A_r = Instantaneous orifice passage area
A_p = Pipe section area
A_w = The water plane area
b = draft
β = Bulk modulus
C = Capacitance
$C_{1,2}$ = DEAP Parameters
C_{dr} = Drag coef?cient
C_v = Viscous drag coefficient
C_f = The flow discharge coefficient
c_g = The group velocity
c_v = The transition approximation coefficient
D_p = Hydraulic pump displacement
E = The magnitude of the electric field
e = The mean wave energy density
e_c = Charging energy
e_{cyc} = Harvested energy in a cycle
e_d = Discharging energy
ε_0 = the permittivity of free space
ε_r = the relative dielectric constant
ε_{33} = Hydrodynamic parameters for the radiation
F_{br} = The breakaway friction force
F_c = The Coulomb friction force
F_D = DEAP reactive force
F_e = The excitation force
F_{el} = Elastic recovering force
F_f = The friction force
F_h = The hydrodynamic force
F_{me} = Maxwell force
F_v = The viscous damping force
F_u = The user's force from PTO system
h = Water depth
η_v = Volumetric efficiency of hydraulic pump
η_t = the total efficiency
I_{fl} = Flywheel inertia
K_{eq} = Equivalent stiffness
k = Wave number

λ = Stretch ratio
λ_w = Wave length
M_a = Added mass
M_b = Buoy mass
M_{eq} = Equivalent mass
M_s = Supplementary mass
N = Number of ADG
n = Pump speed
n_p = Pump speed
p_s = Supplied fluid pressure
p_{pre} = Gas pre-charge pressure
p_{set} = Setting pressure of relief valve
P_w = Mean wave power
Q = Electric charges
Q_d = Discharge flowrate
Q_p = The pump flowrate
Q_r = Flowrate through the relief valve
R_r = Radiation damping coefficient
R_f = Viscous friction coefficient
R_u = User's coefficient
r_h = Flywheel radius
r_{pi} = Pinion radius
ρ = Density of sea water
ρ_h = Density of hydraulic fluid
σ_{me} = Maxwell stress
σ_{el} = Elastic stress
l_0 = Initial length
t = Thickness
S = The active electrode surface
S_h = The hydrostatic stiffness
V_c = Charge voltage
V_{vol} = Volume of DEAP material
V_f = Volume of hydraulic chamber
V_0 = Initial volume of fluid
V_{pre} = Pre-charge volume of gas chamber
ψ = the wave elevation
w_0 = DEAP width
ω = Wave angular frequency
ω_n = PTO natural frequency
ω_p = Pump rotational speed
X_0 = Stretch ratio at equilibrium position
$\ddot{z}(t)$ = Buoy acceleration

1. Introduction

Dielectric elastomers (DE) have been known as suitable candidates for energy harvesting due to some distinct advantages, such as low cost, lightweight, high energy density and good impedance matching to many energy sources.[1] These vibration energy sources include human motion, vehicles, transportation and civil structures which are discussed in Ref. 2. Soft generators using DE is presented by Thomas G. McKay et al. in Ref. 3. Moreover, applications of DE in energy harvesting fields are performed on human passive motion, automobile tires and wave power are reported in Refs. 4-7.

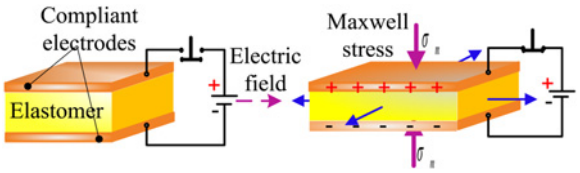

Fig. 1 The basic working principle of DE

A typical DE film includes a soft dielectric elastomer sandwiched between two compliant electrode layers as shown in Fig. 1, and the electroactive nanostructured polymers is reported by Ravi Shankar et al. in Ref. 8. Here, a dielectric elastomer layer is made of a relatively soft polymer such as silicone rubber, and compliant electrode layers are produced by coating carbon grease or the noble metals, such as platinum or gold. DEs have shown potential application in the actuator mode. Recently, the generator mode has gained more attention. In the actuator mode, electrical energy is converted into mechanical work by bringing opposite charges closer together. In the reversely, in the generator mode, mechanical work is converted to electrical energy by amplifying the pre-charged energy.

Some previous works that involve in application and development of DE have been taken into account. For example, the energy gain and other important material parameters are optimized to fit the requirement for energy converter in Ref. 9. A DE generator based on circular energy conversion unit is studied by Huaming W. et al. in Ref. 10 to investigate effect of bias voltage and stretch displacement on the generated energy and efficiency. Jean-Mistral C. et al. in Ref. 11 developed a reliable method for modelling DE generator based on biaxial plane. And, two elementary characteristic dielectric elastomer energy generating synergetic structures (DIESYS) design concepts for in-plane and out-plane oscillations are examined by Anroniadis I. A. et al. in Ref. 12.

Being the group of Electroactive polymers (EAPs) and DE, Dielectric electro-active polymers (DEAP) is made by Danfoss Polypower. DEAP have shown great promise due to their capabilities for high strain and significant change in capacitance. There are some typical studies on this material. Firstly, elastic behavior of DEAP film in the development of actuators is reported in Ref. 13. Next, an analytical model for the electromechanical response of cone DEAP actuators is developed by Y. Zhu in Ref. 14, and hysteresis modeling and identification of DEAP actuator using an APSO based nonlinear Preisach NARX fuzzy model is presented in Ref. 15. In order to investigate the performance of DEAP generator mode in a wave energy converter (WEC), modeling and experimental investigation on DEAP generator is studied in Ref. 16. Moreover, a design and modeling of the antagonistic structure generator is developed in Ref. 17 to increase the conversion energy efficiency in wave energy harvesting application. Finally, based on the reliable analytical model, a design and modeling of an innovative WEC using DEAP is proposed in Ref. 18.

Although previous studies have taken into account valuable results, there are some challenges to face in application of DEAP in generator mode. Among, stretch ratios play important role to optimize the harvested

energy and prevent mechanical breakdown of DEAP generator. Obviously, stretch ratios can be set up in laboratory environment precisely; however, these must be obtained by solving the dynamic performance in the realistic vibration source. For example, when the DEAP generator is applied in the WEC, stretch ratios must be obtained of the hydrodynamic behavior and interaction between the buoy and an incident wave.[18]

This paper investigates the performance of a novel WEC using DEAP generator with optimization stretch ratios. Firstly, modeling of antagonistic DEAP generator (ADG) is introduced. Then, the hydrodynamic model using the linear potential wave theory is presented and validated by experimental results under different wave profiles. Next, the complete analytical model including the hydrodynamic force, due to incident wave, coupled with the electromechanical force, due to DEAP stiffness, is expressed in time domain. Moreover, a variable supplementary inertia (SI) device is attached on the float to control the hydrodynamic performance of the float. The natural frequency of device is controlled by adjusting the SI. Consequently, reacting to the incident wave, the elevations of the float is obtained by solving the hydrodynamic behavior. Based on the float elevations, the response stretch ratios are determined and controlled to reach the desired values under different regular waves (different amplitudes and frequencies). Here, the PID controller is employed to generate the SI of device. Finally, a numerical simulation is built in MATLAB®/Simulink® to investigate performances of WEC under hydrodynamic behavior. By setting some parameters, simulation results indicate that stretch ratios can be controlled to optimize the harvested energy and to satisfy the realistic requirement.

2. Working Principle of DEAP Generator

Several energy cycles were studied in Ref. 19. Based on a constant charge Q, Fig. 2 illustrates basic operating principle of DEAP generator in an energy harvesting. Firstly, DEAP material is pre-stretched in order to decrease the charged voltage and to increase the performance. Then, the mechanical energy is applied to stretch DEAP generator, which causes reduction in thickness and increasing the surface area. Its capacitance is given by the equation:

$$C = \varepsilon_r \varepsilon_0 \frac{S}{t} = \varepsilon_r \varepsilon_0 \frac{V_{vol}}{t^2} \tag{1}$$

After stretch material, a pre – charge $Q = CV_c$ is placed upon the two electrode layers where positive charges are on one side and negative ones are one the other side. Due to the Coulomb's law, an electric field is induced between two electrode layers. Then, the stress due to electrostatic force, as calculated by Krakovesky I. et al. in Ref. 20 can be expressed in Eq. (2). It is assumed that only electrostatic phenomenon is represented.

$$\sigma_{me} = \varepsilon_0 \varepsilon_r E^2 \tag{2}$$

At this moment, the input charged energy into DEAP can be expressed in the following equation:

$$e_1 = 0.5 C_c V_c^2 \tag{3}$$

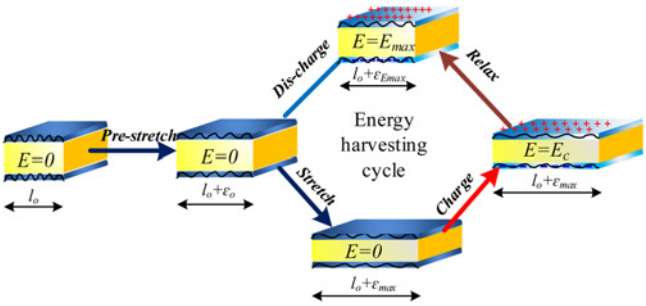

Fig. 2 Basic working principle of DEAP energy cycle

On path 3-4, the DEAP material is allowed to retract point 4 based on the equilibrium between the elastic recovering force and electrostatic force. Then, the stored energy in DEAP at this point is expressed in Eq. (4):

$$e_2 = 0.5 C_d V_d^2 \tag{4}$$

Finally, the output energy of DEAP generator per cycle defined as the difference of Eqs. (4) and (3) is obtained in Eq. (5)

$$e_{cyc} = e_2 - e_1 = 0.5 C_c V_c^2 (C_c/C_d - 1) \tag{5}$$

Here, the second equality can be expanded due to constant charge $Q = CV_c$.

3. Modeling Mechanical Behavior of ADG

In order to describe dynamic behavior of ADG, a complete model including mechanical coupling electrical system is depicted in Fig. 3. Two DEAP generators are antagonistic connection by a cable and pulley system. The reactive force imposed in each DEAP generator consists of the elastic recovering force and Maxwell force. Using the Newton second's law, the dynamic equation of the attached mass motion in term of stretch ratio is expressed in the set of Eq. (6).

$$\begin{aligned} M_{eq} l_0 \frac{d^2 \lambda_z}{dt^2} &= F_h - F_1 + F_2 \\ \lambda_z &= \frac{l_0 + X_0 + z}{l_0} \end{aligned} \tag{6}$$

To determine the reactive force, the Mooney-Rivlin model is employed to describe stretch ratio and force relationship. Stress in term of stretch ratio was given in Ref. 21. Defining λ is stretch ratio of DEAP 1, the elastic recovering force is obtained by multiplying the stress and current section area, and presented in Ref. 16. It is re-written in Eq. (7).

$$F_{el1} = w_0 t_0 \left[2\left(C_1 + \frac{C_2}{\lambda}\right)\left(\lambda - \frac{1}{\lambda^2}\right) \right] \tag{7}$$

And, the Maxwell force is presented in Eq. (8)

$$F_{me1} = \varepsilon_0 \varepsilon_r \frac{w_0 V_c^2 \lambda}{t_0} \tag{8}$$

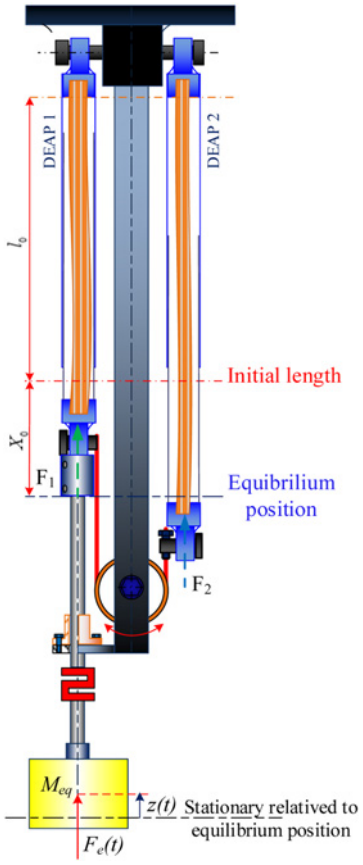

Fig. 3 Schematic of the ECU

Then, the reactive force of DEAP 1 generator is expressed in Eq. (9).

$$F_1 = w_0 t_0 \left[2\left(C_1 - \frac{C_2}{\lambda}\right)\left(\lambda - \frac{1}{\lambda^2}\right)\right] - \varepsilon_r \varepsilon_0 \frac{w_0 V_c^2 \lambda}{t_0} \tag{9}$$

By analogy, the reactive force of DEAP 2 generator is obtained by determining the stretch ratio λ_2 in term of λ. Then, the reactive force of DEAP 2 in term of λ is obtained in Ref. 17 and given in the set of Eq. (10)

$$F_2 = 2w_0 t_0 \left(C_1 - \frac{C_2}{2S_0 - \lambda}\right)\left(2S_0 - \lambda - \frac{1}{(2S_0 - \lambda)^2}\right) - \varepsilon_r \varepsilon_0 w_0 \frac{V_c^2 (2S_0 - \lambda)}{t_0} \tag{10}$$

$$S_0 = (\lambda_2 + \lambda)/2$$

Substituting Eqs. (9) and (10) into Eq. (6), the coupled equation of motion can be obtained as follow:

$$M_a l_0 \ddot{\lambda} + 2w_0 t_0 \left[\left(C_1 + \frac{C_2}{2S_0 - \lambda}\right)\left(2S_0 - \lambda - \frac{1}{(2S_0 - \lambda)^2}\right) - \left(C_1 + \frac{C_2}{\lambda}\right)\left(\lambda - \frac{1}{\lambda^2}\right)\right] + 2\varepsilon_0 \varepsilon_r \frac{w_0 V_c^2}{t_0}(\lambda - S_0) = F_h \tag{11}$$

Material parameters C_1 and C_2 can be determined by curve fitting experiment results with Eq. (11). Identification DEAP material parameters is presented in Ref. 16, and these results are shown in Table 1. Employing the test rig in Fig. 4, the analytical model is validated by

Table 1 the identified DEAP parameters

Parameters	Strecth stroke	Relax stroke
C_1 (Pa)	45202e5	2.5335e5
C_2 (Pa)	-3.526e5	-1.1844e5

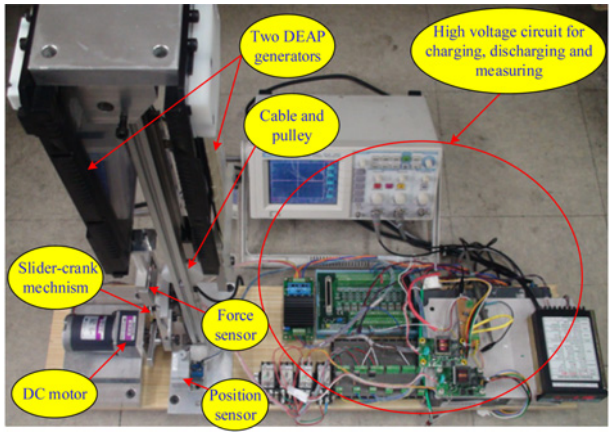

Fig. 4 Test rig of ADG

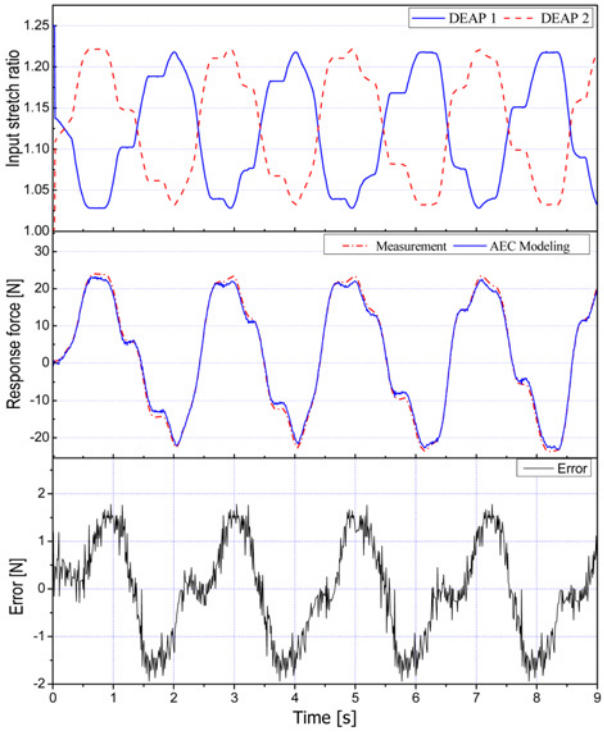

Fig. 5 Relative force error between modeling and measurement with random input stretch ratio

acceptable agreement between simulation results and that of measurement. Fig. 5 illustrates the response forces comparison. The same input stretch ratio is applied to the DEAP generators, the induced forces are measured and compared with the simulation results. It is indicated that the relative error is bounded in 5%.

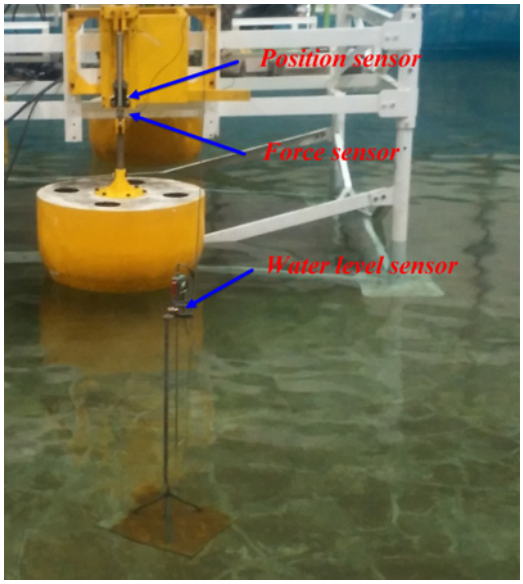

Fig. 6 Test rig for validation of wave buoy interaction in water tank

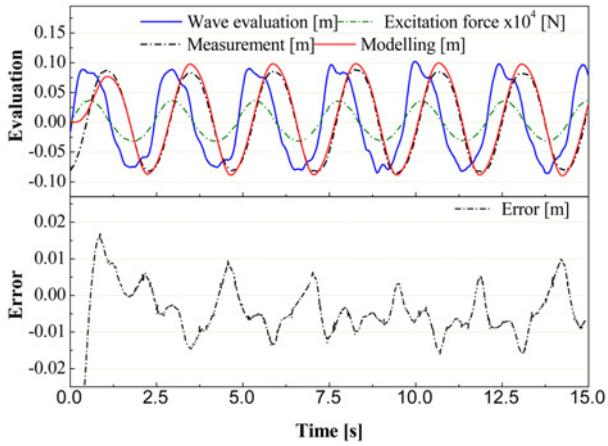

Fig. 7 The buoy elevation comparisons for validation hydrodynamic model in water tank

4. Hydrodynamic Model

In order to investigate hydrodynamic performance of a buoy and wave interaction, a test rig is designed, fabricated and assembled in the Research Institute of Small & Medium Shipbuilding (RIMS). The test layout is shown in Fig. 6. It includes the buoy, the power take-off (PTO) system and the peripheral interface devices. Using the Newton second's law, the acceleration of the buoy in the heave mode is obtained in Eq. (12)

$$\ddot{z} = \frac{F_h + F_u}{M_b} \tag{12}$$

where the hydrodynamic force F_h is calculated in Ref. 22 and presented in the following equation:

$$F_h = F_e + F_r + F_v + F_f + F_s \tag{13}$$

The excitation force is usually decomposed in two components: Froude-Krylove force and the diffraction force. Here, the Froude-Krylove force is caused by the undisturbed wave field and can be represented for the excitation force. The diffraction force can be negligible due to small floating buoy. The excitation force F_e is a function of the amplitude, frequency and phase of waves, and it is given in the following equation:

$$F_e = f_3 A \sin(\omega t + \alpha) \tag{14}$$

where f_3 is the force amplitude, and α is the phase difference between the wave and the excitation force.

The radiation force induced by buoy oscillations is required to move the buoy, and it is obtained in Eq. (15)

$$F_r = -M_a \ddot{z} - R_r \dot{z} \tag{15}$$

where M_a is the added mass at an infinite frequency, and R_r is the radiation damping coefficient.

The viscous damping force induced by relative turbulent flow is calculated by the following equation:

$$F_v = -\frac{1}{2}\rho C_v A_w (\dot{z} - \dot{\psi})|\dot{z} - \dot{\psi}| \tag{16}$$

where C_{dr} is drag coefcient, and A_w is the water plane area of the buoy at rest.

The friction force of the PTO system can be modeled by proposing Armstrong's method in Ref. 23, and approximated with the following equation:

$$F_f = (F_c + (F_{br} - F_c) e^{(-c_v|\dot{z}|)}) sign(\dot{z}) + R_f \dot{z} \tag{17}$$

where F_c is the Coulomb friction which opposes motion with a constant force at any velocity; the breakaway friction force F_{br} is the sum of the Coulomb and static frictions at zero velocity; the transition approximation coefficient c_v is used for the approximation of the transition between the static and the Coulomb frictions.

The hydrostatic restoring force, due to excursion of the buoy from its equilibrium position, can be calculated by using the Archimedes principle, and it is simply given in Eq. (18):

$$F_s = -S_b z \tag{18}$$

The user's force reacting to the PTO is the required force to drive the PTO system. It is usually calculated as follow:

$$F_u = -R_u \dot{z} \tag{19}$$

The equation of motion for the buoy is given in Eq. (12) and rewritten in Eq. (20) by substituting Eqs. (13)~(19) into Eq. (12):

$$\begin{aligned}(M_b + M_a)\ddot{z} + (R_r + R_f + R_u)\dot{z} + S_b z + \frac{1}{2}\rho C_v A_w (\dot{z} - \dot{\psi})|\dot{z} - \dot{\psi}| \\ + (F_c + (F_{br} - F_c) e^{(-c_v|\dot{z}|)}) sign(\dot{z}) = f_3 A \sin(\omega t + \alpha)\end{aligned} \tag{20}$$

5. A Novel Design of a WEC System

5.1 Design concept & working principle

The general conceptual design of the proposed WEC is illustrated in Fig. 8. There are five main components, such as a stationary platform, a variable inertia hydraulic flywheel (VIHF), DEAP transducers, and a

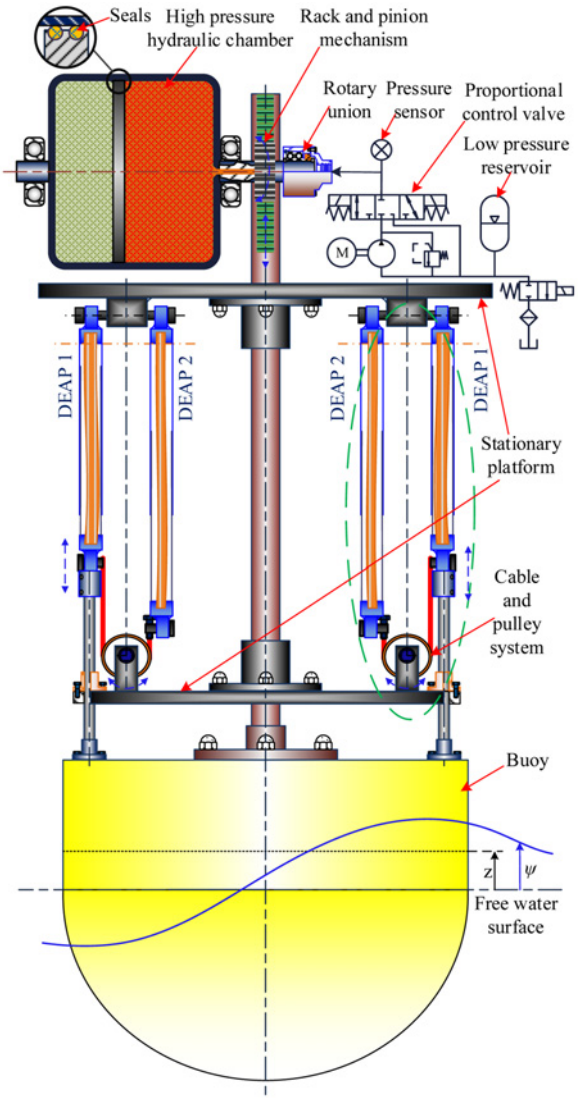

Fig. 8 The proposed WEC including multiple ADG and VIHF

floating buoy and main control unit (MCU). The platform is held stationary relative to free water surface on the sea. The VIHF is mounted on the platform and rotates around its axis. A plurality of DEAP transducers are fixed on the platform at one end and the other ends are fixed on the floating buoy. The main shaft of the buoy is coupled with the VIHF thanks to rack and pinion mechanism. Moreover, the MCU is employed to collect data and send control signal to operate the VIHF.

Reacting to the incident waves, the floating buoy oscillates up and down. Then, DEAP transducers are also stretched and relaxed. Since two DEAP generators are antagonistic connection in each ADG, they are stretched and relaxed inversely. One DEAP generator is stretched, the other DEAP generator is allowed to retract. On the other hand, the elastic force of one DEAP generator in relaxing phase is used to stretch the opposite one. Thus, the required forces using to drive a transducer are reduced in the same stretch ratio. Moreover, for increasing the absorbed energy, the equivalent inertia of floating buoy structure must be tuned to the values which bring the natural frequencies of device to close to wave spectrum frequencies (resonances behavior). The VIHF plays a role as the SI. By controlling fluid inside chamber, mass of the VIHF will be changed to adjust its inertia. Once the SI is changed, the equivalent inertia will be adjusted. Consequently, the buoy elevation (BE) and stretch ratio can be controlled to improve the performance and efficiency of the device.

Compared with previous ideas about controlling SI, this paper shows convenient mechanism to satisfy the realistic requirement of WEC using DEAP. The proposed design keeps the floating buoy closed to the water surface to have good radiation capabilities while it maintains the same draft compared to the adjusted draft in Ref. 18. It is also controllable device compared to two splited bodies in Refs. 24-25, or rigid supplementary mass in Ref. 26.

5.2 Mathematical model

As shown in Fig. 8, a variable SI is taken into account to analyze the combined model of the proposed WEC. The forces acting on the floating buoy consist of the reactive force, the supplementary force and the hydrodynamic force. The resistive force from the PTO involves the force required to drive all ADG. The supplementary force involves change in hydrodynamic performance of the proposed WEC by adjusting the natural frequency. By using the wave linear theory, behavior of the buoy is analyzed as a single body system with one degree of freedom along the vertical z-axis.[22] According to the Newton second's law, the equation of motion of the buoy is obtained in Eq. (21):

$$\ddot{z} = \frac{F_h + F_D + F_{sup}}{M_b} \tag{21}$$

$$F_D = NK_{eq}z \tag{22}$$

$$F_{sup} = -\frac{I_{fl}\ddot{\theta}}{r_p} = -\frac{I_{fl}\ddot{z}}{r_p^2} \tag{23}$$

Substituting Eqs. (13), (22) and (23) into Eq. (21), the complete motion equation of floating buoy is expressed in Eq. (24):

$$\begin{aligned}&(M_b + M_a + I_{fl}/r_p^2)\ddot{z} + (R_r + R_f + R_u)\dot{z} + (S_b + NK_{eq})z \\ &+ \frac{1}{2}\rho C_v A_w(\dot{z} - \dot{\psi})|\dot{z} - \dot{\psi}| + (F_c + (F_{br} - F_c)e^{(-c_v|\dot{z}|)})sign(\dot{z}) \\ &= f_3 A\sin(\omega t + \alpha)\end{aligned} \tag{24}$$

5.3 Optimum SI

For the given buoy and the given incident wave, the absorbed energy can be maximized by bringing the natural frequency of the PTO devices ω_n close to wave excitation frequency ω (resonance behavior).[22] This can be achieved by attaching an adaptive SI:

$$\omega_n \equiv \sqrt{\frac{S_b + NK_{eq}}{M_b + M_a + I_{fl}/r_p^2}} = \omega \tag{25}$$

Then, the optimum SI of the flywheel is obtained

$$I_{fl} = r_p^2\left[\frac{(S_b + NK_{eq})}{\omega^2} - M_b - M_a\right] \tag{26}$$

K_{eq} is the equivalent stiffness of the ADG, and it is defined as follow:

$$K_{eq} = \frac{abs(F_1 - F_2)}{z} \tag{27}$$

However, due to limitation of stretch ratio for mechanical breakdown

strength of DEAP. The optimum SI must be derived to satisfy the desired values.

5.4 Modeling of variable inertia hydraulic flywheel

The current inertia of the hydraulic flywheel includes the initial inertia without fluid and the inertia of fluid pumped into hydraulic chamber, and it is expressed in Eq. (28):

$$I_{fl} = I_i + I_f = I_i + \frac{\rho V_f r_h^2}{2} \tag{28}$$

The fluid inside the accumulator is a function of the supplied hydraulic pressure, pre-charged pressure, accumulator capacity and specific heat ratio. It is calculated by the following:

$$V_f = \begin{cases} 0, & if \quad P_S \le P_{pre} \\ V_{pre}\left[1-\left(\frac{P_{pre}}{P_S}\right)^{\frac{1}{n}}\right], & if \quad P_S > P_{pre} \end{cases} \tag{29}$$

Here, the pressure inside the flywheel-accumulator is calculated by the continuity equation:

$$\frac{dP_s}{dt} = \frac{\beta}{(V_f + V_0)}(Q_p - Q_d - Q_r) \tag{30}$$

The pump flowrate Q_p is calculated as:

$$Q_p = \eta_v D \omega_p \tag{31}$$

The discharge flowrate is depended on the value of current fluid pressure P_S and can be obtained as:

$$Q_d = C_d A_p \sqrt{\frac{2P_S}{\rho}} \tag{32}$$

The flowrate going through the relief valve is calculated as:

$$Q_r = \begin{cases} 0, & if \quad P_S \le P_{set} \\ C_{dr} A_r \sqrt{\frac{2(P_S - P_{set})}{\rho}} & if \quad P_S > P_{set} \end{cases} \tag{33}$$

6. Control Strategy

For controlling of the stretch ratio, the flowchart control is proposed in Fig. 10. For the given wave profiles and specifications of the PTO system, the hydrodynamic parameters are pre-computed by WAMIT software.[27] An analytical model is built to investigate the BE. The responded stretch ratio is obtained in term of the BE. Stretch ratio closed-loop control is applied to generate the required SI. Here, the relative error between desired stretch ratio and actual stretch ratio is sent to the controller. The controller sends the output signal to generate the required inertia of the VIHF. The supplementary mass is calculated and sent to the analytical model.

WEC using DEAP is very complex to build the transfer function or state-space observer. The nonlinearities are mainly caused by flow-pressure characteristics of hydraulic system, viscous friction of hydrodynamic and mechanical behaviour of DEAP. In this study, a proportional flow control valve is employed to adjust flow rate of the VIHF. Once the supplying pressure is adjusted, it will change the

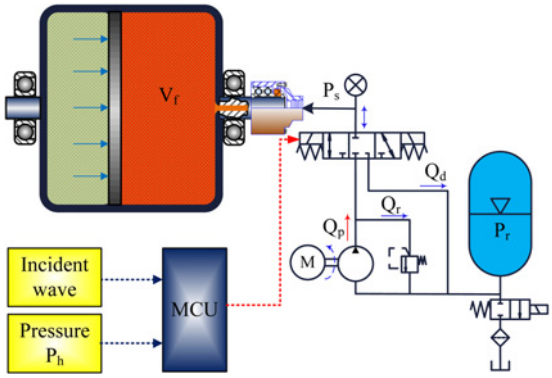

Fig. 9 Specification of the VIHF with hydraulic circuit

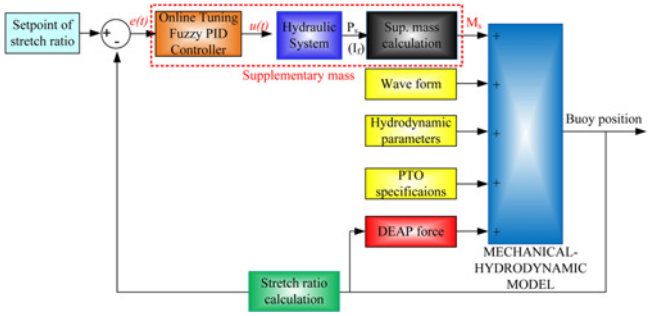

Fig. 10 Schematic control diagram for stretch ratio

performance of the proposed WEC. PID controller is often used due to its simple structure and easy design. The control signal $u(t)$ is expressed in the time domain as follow:

$$u(t) = K_P e(t) + K_I \int_0^t e(t)dt + K_D \frac{de(t)}{dt} \tag{34}$$

where $e(t)$ is the error between the desired stretch ratios and the measured values, K_P is the proportional gain, K_I is the integral gain and K_D is the derivative gain.

7. Energy Conversion Efficiencies

For a given regular wave, the mean wave power is given in Ref. 22. It is a function of the mean wave energy density per unit horizontal area and the group velocity. And, the mean wave power are expressed in the set of Eq. (35):

$$\begin{aligned} P_w &= e c_g, \quad (kW/m) \\ e &= e_k + e_p = \frac{1}{8}\rho g^2 H^2, \quad (J/m^2) \end{aligned} \tag{35}$$

For constant water depth h, the group velocity is given in Ref. 22 and expressed in the set of Eq. (36):

$$\begin{aligned} c_g &= \frac{D(kh)}{2\tanh(kh)} c_p = \frac{g}{2\omega} D(kh) \\ D(kh) &= \left[1 + \frac{2kh}{\sinh(2kh)}\right]\tanh(kh) \\ k &= 2\pi/\lambda \end{aligned} \tag{36}$$

Table 2 Specification of DEAPs generator

Parameters	Value
t_0	80×10^{-6} m
w_0	2 m
l_0	0.18 m
ε_0	8.85×10^{-12} F/m
ε_r	3.1
E_{max}	40×10^{6} V/m
DEAPs mass	0.0297 kg

Table 3 Parameters for working conditions

Parameters	Value
Operating environment	Dry environment
Operating frequency	0.5 Hz
Sampling time	0.01 s
Maximum stretch ratio	122.5%
m_{eq}	0.7 kg
V_c	1300 V
Gravitational acceleration	9.81 m/s^2

Table 4 Wave profile and PTO's parameters for simulation

Parameters	Value
a	0.25 m
h	1.2 m
Case 1: ψ_1	0.005sin(2.244t) m
Case 2: ψ_2	0.004sin(πt) m

where $D(kh)$ is the depth function.

Time dependency of mean wave power of an incident wave is calculated by integrating Eq. (35) over time domain:

$$e_w = \int_0^t P_w, \quad (J) \tag{37}$$

In analogy with Eq. (37), the harvested energy is obtained by integrating Eq. (5) over time domain:

$$e_{har} = \int_0^t e_{cyc}, \quad (J) \tag{38}$$

Finally, the total efficiencies of the proposed WEC defined by ratio results of Eqs. (38) and (37) is calculated by Eq. (39):

$$\eta_t = \frac{e_{har}}{e_w} \tag{39}$$

8. Simulation Results and Discussions

Before investigating the performance of the proposed WEC, some parameters must be prescribed in advance. Here, Specifications of DEAP generator is given by Danfoss PolyPower and shown in Table 2. Table 3 shows working conditions. The wave profiles and specification of the floating buoy are shown in Table 4. And, hydrodynamic parameters are obtained by using WAMIT software and plotted in Fig. 11.

Numerical model is built in MATLAB®/Simulink®. Then, two types of simulations are carried out to investigate the performance. The first type involves in response of the proposed WEC with different SI separately. The second type involves in response of the WEC device with stretch ratio closed loop control.

In the first type of simulation, the performance of WEC is investigated

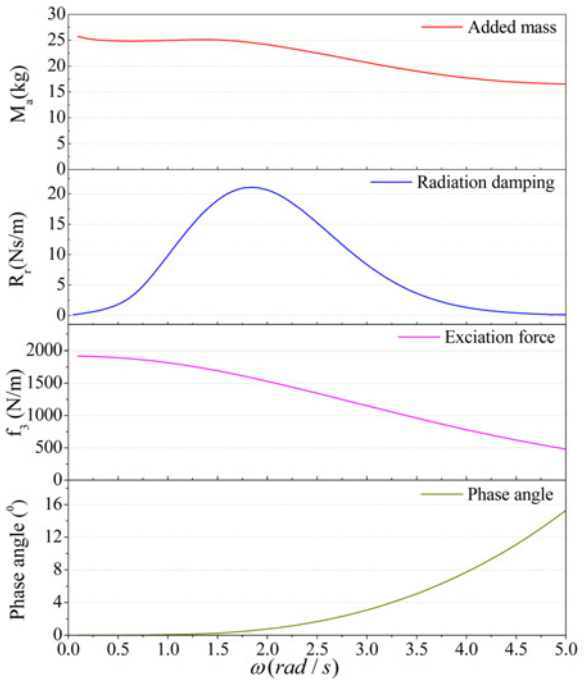

Fig. 11 Hydrodynamic parameters for the heave mode of the floating truncated vertical cylinder of radius a=0.5 m and of draft b=0.5 m in water of depth h=1.2 m

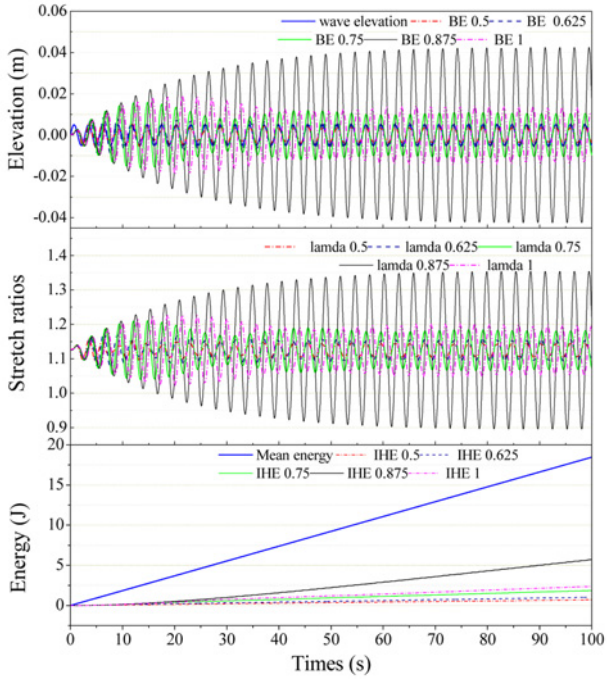

Fig. 12 Change in BE, stretch ratio and total theoretical harvested energy for various SI: 0.5 kgm^2, 0.625 kgm^2, 0.75 kgm^2, 0.875 kgm^2 and 1 kgm^2 under wave profile ψ_1

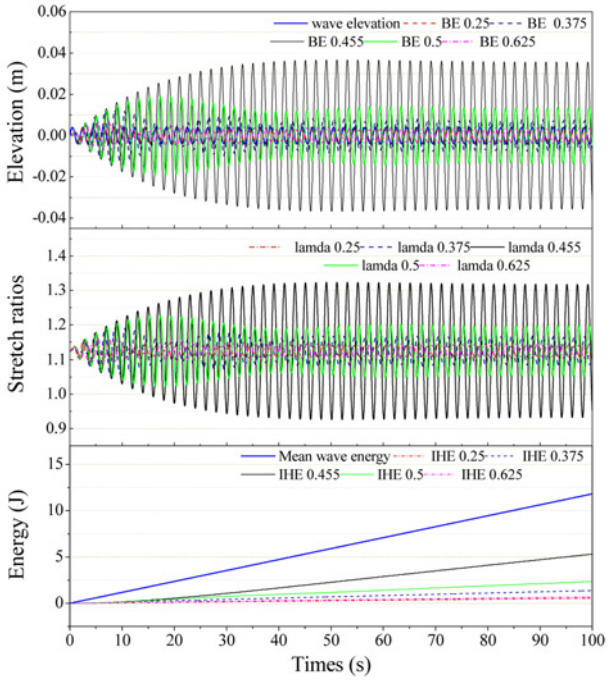

Fig. 13 Change in BE, stretch ratio and total theoretical harvested energy for various equivalent mass at 0.25 kgm^2, 0.375 kgm^2, 0.455 kg, 0.5 kgm^2 and 0.625 kgm^2 under wave profile ψ_2

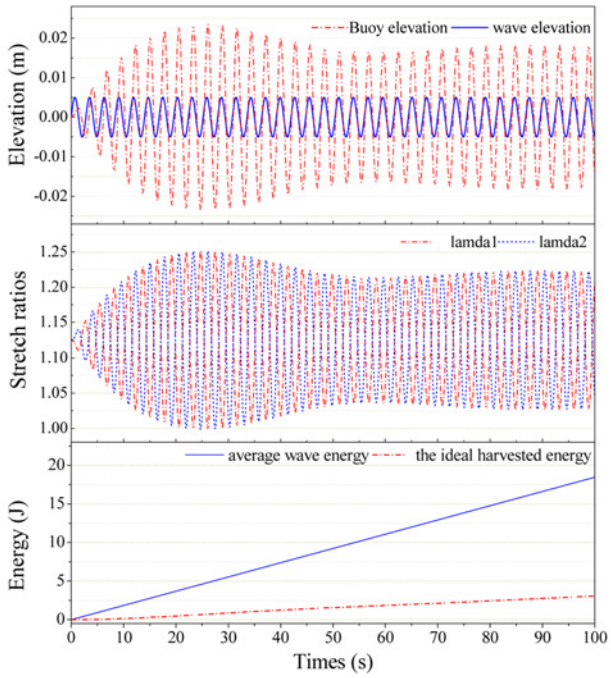

Fig. 14 Ideal performance of the proposed WEC under case 1 of wave ψ_1 at SI=0.875 kgm^2

in two regular waves and different SI. Simulation results are plotted in Figs. 12 and 13 with case 1 and case 2 of waves, respectively. In the Fig. 12, the BE under changing in SI are shown on the top part. Response stretch ratios and harvested energy are shown in the middle and bottom part, respectively. Similar to results in Fig. 12, Fig. 13 plots simulation results for changing SI from 0.25 to 0.625 kgm^2 with step 0.125 kgm^2 under case 2 of wave. It is cleared that resonance behavior can be found at SI_1 = 0.875 kgm^2 and SI_2 = 0.455 kgm^2 with case 1 and case 2 of wave, respectively. The BE and stretch ratios are increasing at these points significantly. In theoretical vibration, this can be reasonable. However, due to limitation of stretch ratio for mechanical breakdown, the SI must be selected to satisfy maximum stretch ratio in the steady state. After two optimum SI are selected to generate the desired stretch ratio, the responses of WEC are plotted in Figs. 14 and 15. As shown, although stretch ratios are reaching the desired stretch ratio at the steady state, large overshoot happen at the transient state. These point can cause damage to DEAP material because of mechanical breakdown strength.

In order to eliminate the large overshoot at the transient state, stretch ratio closed loop control is applied improve the performance of the WEC. Then, the simulation results are shown in Figs. 16 and 17 with case 1 and case 2 of wave, respectively. In this work, the desired stretch ratio of DEAP material is about 1.22. The stretch ratios are reaching to desired stretch ratio without overshoot. The response of WEC system is also smooth.

Moreover, it takes a little time from transient states to the steady-state because these are strongly dependent on difference between wave elevations and desired stretch ratios. In addition, the hydraulic system and the controller have significant influence on SI which have been

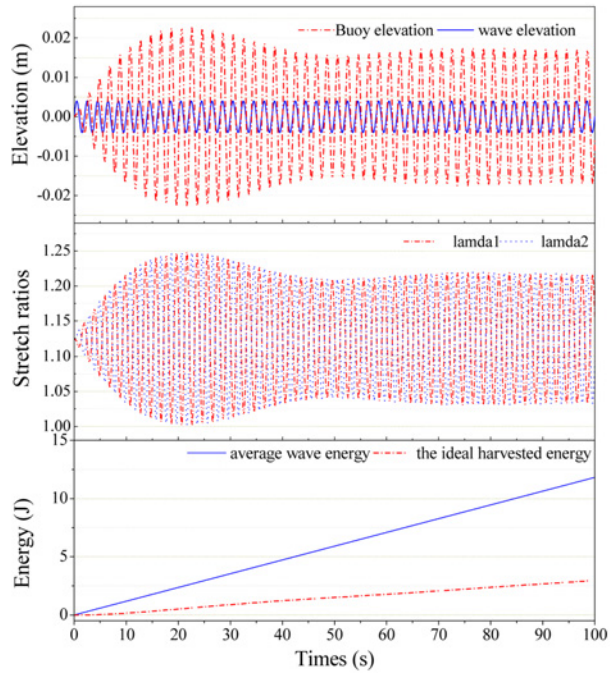

Fig. 15 Ideal performance of the proposed WEC harvested energy in 25% efficiency under case 2 of wave ψ_2 at SI=0.455 kgm^2

taken into account to change the hydrodynamic performance of the WEC device. Fortunately, the transient times are so small compared with the working time of WEC device, and wave spectrum is only changed several times a day. Therefore, the proposed WEC can shows its advantage for realistic application.

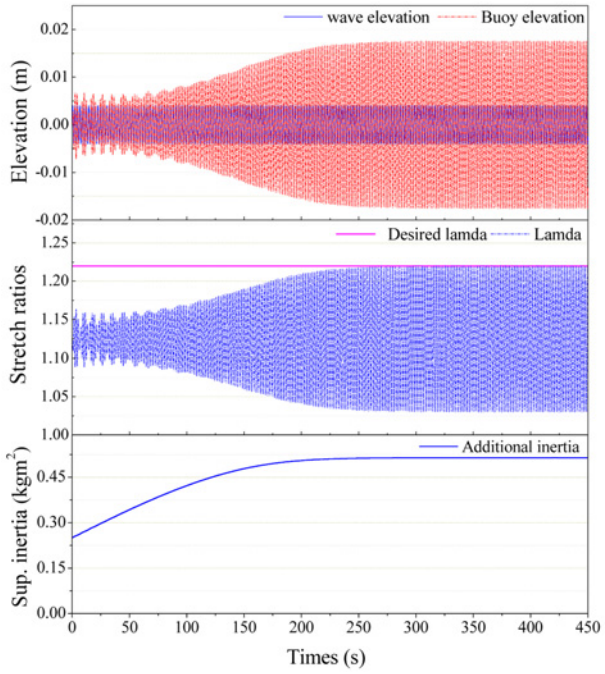

Fig. 16 Response to optimum control for stretch ratio under case 1 of wave

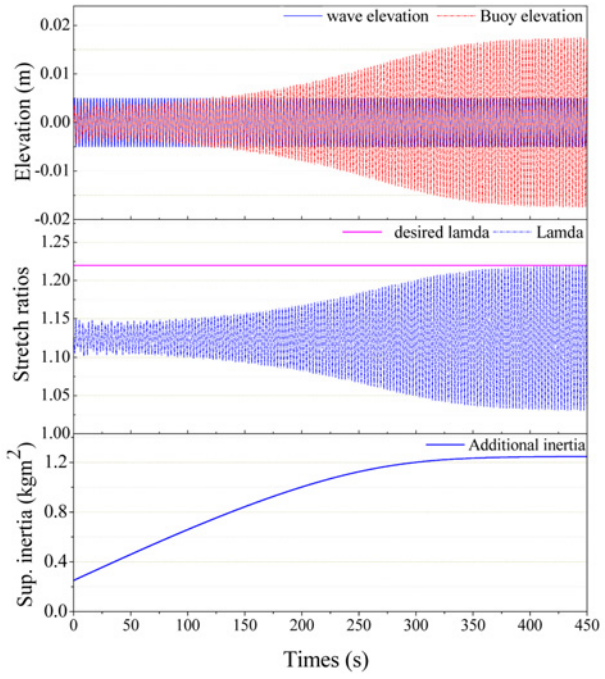

Fig. 17 Response to optimum control for stretch ratio under case 2 of wave

9. Conclusion and Future Works

This paper improves the performance of a novel WEC using DEAP generator. The complete analytical model including the hydrodynamic force, due to incident wave, coupled with the electromechanical force, due to DEAP stiffness, is simulated by using MATLAB®/Simulink® in time domain. Here, modeling of the ADG is introduced, and the hydrodynamic model using the linear potential wave theory is presented and verified by experimental results under different wave profiles. The VIHF is proposed to control SI which adjust the natural frequency of WEC device. Stretch ratios closed loop control is applied by using the PID controller to reach the desired values under different regular waves (different amplitudes and frequencies). Consequently, simulation results indicate that the overall energy conversion efficiency of the proposed WEC can reach up to 25% and the response of WEC device is improved significantly.

This model can be proposed to adapt to any DE materials which have larger strain capacity and higher energy density. A complete test rig will be deployed at RIMS in future project to validate the proposed WEC with experimental results. Moreover, investigation of the performance in the irregular waves can be studied to satisfy the realistic requirement of the proposed WEC.

ACKNOWLEDGEMENT

This work was supported by the New & Renewable Energy of the Korea Institute of Energy Technology Evaluation and Planning (KETEP) grant funded by the Korea government Ministry of Trade, Industry and Energy (G031518511).

REFERENCES

1. Pelrine, R., Kornbluh, R. D., Eckerle, J., Jeuck, P., Oh, S., et al., “Dielectric Elastomers: Generator Mode Fundamentals and Applications,” Proc. of SPIE's 8th Annual International Symposium on Smart Structures and Materials, Vol. 4329, pp. 148-156, 2001.
2. Zuo, L., and Tang, X., “Large-Scale Vibration Energy Harvesting,” Journal of Intelligent Material Systems and Structures, Vol. 24, No. 11, pp. 1405-1430, 2013.
3. McKay, T. G., O’Brien, B. M., Calius, E. P., and Anderson, I. A., “Soft Generators using Dielectric Elastomers,” Applied Physics Letters, Vol. 98, No. 14, Paper No. 142903, 2011.
4. Abdi, H., Mohajer, N., and Nahavandi, S., “Human Passive Motions and a User-Friendly Energy Harvesting System,” Journal of Intelligent Material Systems and Structures, Vol. 25, No. 8, pp. 923-936, 2014.
5. van den Ende, D. A., Groen, W. A., and van der Zwaag, S., “Robust Piezoelectric Composites for Energy Harvesting in High-Strain Environments,” Journal of Intelligent Material Systems and Structures, Vol. 24, No. 18, pp. 2262-2269, 2013.
6. Ahnert, K., Abel, M., Kollosche, M., Jørgensen, P. J., and Kofod, G., “Soft Capacitors for Wave Energy Harvesting,” Journal of Materials Chemistry, Vol. 21, No. 38, pp. 14492-14497, 2011.
7. Chiba, S., Waki, M., Wada, T., Hirakawa, Y., Masuda, K., and Ikoma, T., “Consistent Ocean Wave Energy Harvesting using

Electroactive Polymer (Dielectric Elastomer) Artificial Muscle Generators," Applied Energy, Vol. 104, pp. 497-502, 2013.

8. Shankar, R., Ghosh, T. K., and Spontak, R. J., "Electroactive Nanostructured Polymers as Tunable Actuators," Advanced Materials, Vol. 19, No. 17, pp. 2218-2223, 2007.
9. Graf, C., Hitzbleck, J., Feller, T., Clauberg, K., Wagner, J., et al., "Dielectric Elastomer–based Energy Harvesting: Material, Generator Design, and Optimization," Journal of Intelligent Material Systems and Structures, Vol. 25, No. 8, pp. 951-966, 2014.
10. Wang, H., Zhu, Y., Wang, L., and Zhao, J., "Experimental Investigation on Energy Conversion for Dielectric Electroactive Polymer Generator," Journal of Intelligent Material Systems and Structures, Vol. 23, No. 8, pp. 885-895, 2012.
11. Jean-Mistral, C., Basrour, S., and Chaillout, J., "Modelling of Dielectric Polymers for Energy Scavenging Applications," Smart Materials and Structures, Vol. 19, No. 10, Paper No. 105006, 2010.
12. Antoniadis, I. A., Venetsanos, D. T., and Papaspyridis, F. G., "DIESYS—Dynamically Non-Linear Dielectric Elastomer Energy Generating Synergetic Structures: Perspectives and Challenges," Smart Materials and Structures, Vol. 22, No. 10, Paper No. 104007, 2013.
13. Zhu, Y., Zhou, H., and Wang, H., "Electromechanical Characteristic Analysis of a Dielectric Electroactive Polymer (DEAP) Actuator," Smart Materials and Structures, Vol. 24, No. 10, Paper No. 105015, 2015.
14. Usha, S. and Sreekumar, M., "Elastic Behaviour of Deap Film in the Development of Actuators," Procedia Engineering, Vol. 41, pp. 1154-1161, 2012.
15. Truong, B. N. M., Nam, D. N. C., and Ahn, K. K., "Hysteresis Modeling and Identification of a Dielectric Electro-Active Polymer Actuator using an Apso-based Nonlinear Preisach NARX Fuzzy Model," Smart Materials and Structures, Vol. 22, No. 9, Paper No. 095004, 2013.
16. Binh, P. C., Nam, D. N. C., and Ahn, K. K., "Modeling and Experimental Investigation on Dielectric Electro-Active Polymer Generator," Int. J. Precis. Eng. Manuf., Vol. 16, No. 5, pp. 945-955, 2015.
17. Binh, P. C., Nam, D. N. C., and Ahn, K. K., "Modeling and Experimental Analysis of an Antagonistic Energy Conversion using Dielectric Electro-Active Polymers," Mechatronics, Vol. 24, No. 8, pp. 1166-1177, 2014.
18. Binh, P. C., Nam, D. N. C., and Ahn, K. K., "Design and Modeling of an Innovative Wave Energy Converter using Dielectric Electro-Active Polymers Generator," Int. J. Precis. Eng. Manuf., Vol. 16, No. 8, pp. 1833-1843, 2015.
19. Lallart, M., Cottinet, P.J., Guyomar, D., and Lebrun, L., "Electrostrictive Polymers for Mechanical Energy Harvesting," Journal of Polymer Science Part B: Polymer Physics, Vol. 50, No. 8, pp. 523-535, 2012.
20. Krakovský, I., Romijn, T., and de Boer, A. P., "A Few Remarks on the Electrostriction of Elastomers," Journal of applied physics, Vol. 85, No. 1, pp. 628-629, 1999.
21. Martins, P., Natal Jorge, R. M., and Ferreira, A. J. M., "A Comparative Study of Several Material Models for Prediction of Hyperelastic Properties: Application to Silicone-Rubber and Soft Tissues," Strain, Vol. 42, No. 3, pp. 135-147, 2006.
22. Falnes, J., "Ocean Waves and Oscillating Systems: Linear Interactions including Wave-Energy Extraction," Cambridge University Press, pp. 1-275, 2004.
23. Armstrong B. and Canudas de Wit C., "Friction Modeling and Compensation," CRC Press, pp. 1369-1382, 1996.
24. Alves, M., Traylor, H., and Sarmento, A., "Hydrodynamic Optimization of a Wave Energy Converter using a Heave Motion Buoy," Proc. of the 7th European Wave and Tidal Energy Conference, pp. 11-14, 2007.
25. Bozzi, S., Miquel, A. M., Antonini, A., Passoni, G., and Archetti, R., "Modeling of a Point Absorber for Energy Conversion in Italian Seas," Energies, Vol. 6, No. 6, pp. 3033-3051, 2013.
26. Vantorre, M., Banasiak, R., and Verhoeven, R., "Modelling of Hydraulic Performance and Wave Energy Extraction by a Point Absorber in Heave," Applied Ocean Research, Vol. 26, No. 1, pp. 61-72, 2004.
27. WAMIT, Inc., "User Manual Version 7," http://www.wamit.com/manual.htm (Accessed 7 JUL 2016)